Activation of Pd/SSZ-13 catalyst by hydrothermal aging treatment in passive NO adsorption performance at low temperature for cold start application

YoungSeok Ryou [a], Jaeha Lee [a], Sung June Cho [b], Hyokyoung Lee [c], Chang Hwan Kim [c], Do Heui Kim [a,*]

[a] School of Chemical and Biological Engineering Institute of Chemical Processes, Seoul National University, Seoul 151-744, Republic of Korea
[b] Clean Energy Technology Laboratory and Department of Applied Chemical Engineering, Chonnam National University, Gwangju 500-757, Republic of Korea
[c] Hyundai-Kia Motors R&D Center, Hwaseong, 445-706 Republic of Korea

A B S T R A C T

Pd/SSZ-13 catalysts after hydrothermal aging (HTA) treatment at $750\,^\circ C$ for 25 h showed enhanced passive NO adsorption performance at temperature below $120\,^\circ C$, which will be suitable for cold start application, although those calcined at $500\,^\circ C$ did not possess good NO adsorption capacity irrespective of the preparation methods such as incipient wetness impregnation, wet impregnation, ion-exchange, and solid state ion exchange. NO adsorption ability of HTA treated Pd/SSZ-13 samples increases gradually as a function of the metal content, up to 2 wt% Pd loading, and then decreased implying that there is an optimum chemistry between the metal and zeolite support. Combined H_2-TPR and Pd XAFS results clearly demonstrate that PdO mainly existed over the fresh samples, whereas HTA treated samples contained ionic Pd^{2+} species, indicating the redistribution of PdO into highly dispersed Pd^{2+} species within the SSZ-13 structure arising from HTA treatment. Such phenomenon was visually confirmed by comparative STEM-EDS analysis of fresh and HTA Pd/SSZ-13 samples. DRIFT results display the formation of two nitrosyl complexes adsorbed on Pd^{2+} ions, which are directly related to two desorption peaks of NO_x at 250 and $400\,^\circ C$. All combined results provide the unambiguous evidence about the generation of Pd ions in SSZ-13 zeolite induced by HTA treatment, which play as the active sites for NO adsorption at low temperature.

© 2017 Elsevier B.V. All rights reserved.

1. Introduction

As the stringent legislation on NO_x emission is continuously issued and enforced, the removal of NO_x in automotive exhaust from lean-burn engine is considered as a great challenge. In order to reduce NO_x in exhaust gas, selective catalytic reduction (SCR) or NO_x storage reduction (NSR) systems have been applied for several decades. However, since SCR or NSR system cannot operate properly below $200\,^\circ C$, in other words, during cold start period (initial ca. 100–200 s of engine operation), the significant amount of NO_x is released into atmosphere without any catalytic treatment [1]. Therefore, NO_x emission during cold start period must be addressed to fulfill the current and future stringent regulation.

Recently, a novel approach is emerging to reduce NO_x in a cold start emission with the purpose of adsorbing NO_x at low temperature temporarily and releasing them at higher temperature, where the temperature is high enough for SCR or NSR to operate. It was reported that Ce-based material can adsorb NO_x at low temperature (below $200\,^\circ C$). However, facile sulfur poisoning of ceria make it difficult to apply to the practical conditions [2]. Therefore, Pd supported on zeolite attracts considerable attention as a promising material of a cold start NO_x trap catalyst due to its high tolerance against sulfur [2]. In addition, Three-way catalyst including Pd/ZSM-5 as a NO_x storage material is also reported by Honda [3].

Ogura et al. reported that in the CH_4 SCR of NO reaction, the active sites of Pd/ZSM-5 is Pd^{2+} ion species which can adsorb NO and react with CH_4, thus suggesting that the nature of Pd plays a key role in NO adsorption [4]. Moreover, previous reports using NO as prove molecule demonstrated that Pd ion and metallic Pd species can adsorb NO, although PdO cannot [4–9]. Thus, under the highly oxidizing condition like diesel emission, ionic Pd species in

zeolite seem to be an essential component for NO_x adsorption. Chen et al. [2] reported that Pd/CHA has desirable NO adsorption ability at low temperature after comparing various zeolite supports such as CHA, MFI and BEA. Considering the synthesis method of Pd/CHA, the ion exchange of Pd^{2+} ion (0.86 Å) in SSZ-13 is expected to be difficult because of the hydrolysis of Pd ion in aqueous solution and small pore size (3.8 Å) of CHA structure. However, note that Chen et al. [2] demonstrated the presence of Pd ion in HTA treated Pd/zeolite prepared by incipient wetness impregnation which is not a common method for ion exchange, so that the effect of HTA treatment on the NO adsorption capacity and the physicochemical property of Pd/zeolite remains as a big question.

Hence, we extensively investigated the NO adsorption/desorption ability, the behavior, and the active sites of various Pd/SSZ-13 samples prepared by incipient wetness impregnation, wet impregnation, ion-exchange, and solid-state ion exchange. Especially, we focused on the physicochemical change of Pd in Pd/SSZ-13 before and after hydrothermal aging treatment by applying combined XRD, H_2-TPR, XAFS, and DRIFT analysis.

2. Experimental

2.1. Catalysts preparation

NH_4-SSZ-13, obtained from Zeolyst, was used as a support without further treatment. The Si to Al ratio of SSZ-13 is 22.4 (i.e. Si/Al_f: 22.4, Al_f: Framework Al). $Pd(NO_3)_2 \cdot 2H_2O$ (Sigma Aldrich) or $PdCl_2$ (Alfa Aesar) were used as Pd precursor depending on the preparation methods. Four methods including incipient wetness impregnation (IWI), wet impregnation (WET), ion exchange (ION), and solid-state ion exchange (S–S) were applied to load Pd into NH_4-SSZ-13. IWI method used the aqueous $Pd(NO_3)_2$ solution equivalent to the total pore volume of NH_4-SSZ-13. WET method was applied by mixing an excess of aqueous $Pd(NO_3)_2$ solution (200 ml, 5 mM) with 5 g of NH_4-SSZ-13 for 1 h, followed by the evaporation of solvent in a rotary evaporator for 24 h. In case of ION method, 2 g of NH_4-SSZ-13 was introduced into aqueous $Pd(NO_3)_2$ solution (50 ml, 20 mM) and then stirred at 65 °C for 20 h. The filtered solid was washed with DI-water. For S–S method, $PdCl_2$ and SSZ-13 was ground together in a mortar for 1 h. 2 wt% of Pd was loaded on SSZ-13 by using four methods. Furthermore, to investigate the effect of Pd loading, Pd/SSZ-13 catalysts with various Pd loadings (0.2, 0.5, 1, 2, 3, and 5 wt%) were synthesized by applying IWI method. After loading Pd, all catalysts were dried at 105 °C for 24 h and calcined at 500 °C in 15% O_2 balanced with N_2 for 2 h, which were designated as "fresh". In order to investigate hydrothermal stability, the calcined samples were treated with 15% O_2 and 10% H_2O in N_2 (total flow rate: 200 ml/min) at 750 °C for 25 h, which were denoted to "hydrothermal aging (HTA)" samples. Note that there is no Pd loss within the error in Pd/SSZ-13 during HTA treatment, which is verified by ICP measurement before after HTA treatment (ex) Pd(1)/SSZ-13 IWI: As synthesized (1.11 wt%), Fresh (0.94 wt%), and HTA (0.97 wt%).

2.2. Catalysts characterizations

Information about the crystalline structure of the fresh and HTA catalysts was obtained from powder X-ray diffraction (XRD) using a Rigaku (mode 1 smartlab) diffractometer with Cu Ka radiation (40 kV and 30 mA). The XRD patterns were collected in the range of 5–90° (2 θ) with a step size of 0.02° at a speed of 2.5°/min.

X-ray photoelectron spectroscopy (XPS) spectra were collected using a VG Multilab2000 spectrometer (ThermoVG Scientific) equipped with Al Kα (hν = 1486.6 eV) radiation sources. The vacuum pressure of the chamber during XPS analysis was about 10^{-9} Pa. To calibrate the shift due to the charging, the C 1 s binding energy (284.8 eV) was used as a reference.

Cryo-H_2-temperature programmed reduction (Cryo-H_2-TPR) was carried out by using a BEL-CAT-II (BEL Japan Inc.) with a thermal conductivity detector (TCD). 0.05 g of sample was oxidized in a flow of 21% O_2/N_2 at 300 °C for 1 h prior to the measurement. After pretreatment, the sample was cooled down to −90 °C and exposed to 5% H_2/Ar. Temperature was raised from −90 to 900 °C at a rate of 10 °C/min.

Pd K-edge X-ray absorption fine structure (XAFS) of the catalyst was collected in ambient condition at Pohang Accelerator Laboratory (7D-XAFS beamline in PLS-II) using Si(111) crystal as monochromator where the beam energy and ring current were 2.5 GeV and 300 mA, respectively. Energy calibration was carried out for the samples by the Pd foil (E_0 = 24,350 eV). X-ray intensity for Pd K-edge signal was monitored by using ionization chambers purged with pure N_2 gas at room temperature for the measurement of incident (I_0) and fluorescence (I_f) beam. Bulk PdO was used as reference compounds. The step and duration time for X-ray absorption near edge structure (XANES) and extended X-ray absorption fine structure (EXAFS) were 1.0 eV and 2 s, and 0.30 nm^{-1} and 3 s, respectively. The total number of points per XAFS spectrum was 478, sufficient for the analysis of EXAFS. The obtained EXAFS data were analyzed by ATHENA and ARTEMIS.

For XAFS analysis, Artemis implemented in Demeter program package (0.9.25) was utilized after the data processing using Athena. The background removal was performed to extract XAFS signal using AUTOBK program for R_{bkg} = 0.1 nm and subsequently the corresponding XAFS data in k space was fourier transformed with the Kaiser-Bessel window function, 10 nm^{-1} after k^3 weighting to amplify the high k information. The range for fourier transformation for Pd samples, Δk were 30–130 nm^{-1}. The phase shifts and amplitude functions of the reference was generated using $Feff$6L. The curve fitting range in r space, Δr was varied depending on the sample. The number of independent point of the data for the curve fit, N_{idp} determined from Nyquist theorem was always larger than the number of variable, providing the sufficient degree of freedom, N_{var}. The scattering path from the possible model structure was obtained from the $Feff$ calculation. Only scattering with large contribution were included in the multi-shell fitting. The many-body reduction factor, S_0^2 for Pd, 0.9 was obtained from the curve fit of the XAFS data of Pd foil under the same condition and utilized further in the curve fit of the sample. The statistical quality of the curve fit or proposed model can be determined from the R-factor available in the refinement.

Scanning transmission electron microscopy (STEM) and Energy-dispersive spectroscopy (EDS) analysis was carried out at an accelerating voltage of 200 kV in a JEM-2100F (JEOL) electron microscope equipped with Field emission gun. EDS mapping analysis was conducted on more than ten particles. By applying low dwell time and averaging over several accumulations, the beam damage of samples was minimized. During the scanning, beam tracking was used to avoid drift. All STEM specimens were suspended in ethanol and then ultrasonically dispersed. Drops of the suspension were fully deposited onto a copper grid coated with carbon and then dried overnight before analysis.

DRIFT spectra were acquired in the range of 4000–600 cm^{-1} with 128 scans at a resolution of 4 cm^{-1} on a Nicolet 6700 (Thermo Fisher Scientific) with a MCT detector using DRIFT cell (HARRIC praying mantis^{TM}). Before NO adsorption with 100 ppm NO, 2.5% H_2O, 9.5% O_2 in N_2 balance (200 ml/min), the pretreatment was conducted without NO at 500 °C for 30 min to remove impurities. After NO adsorption at 120 °C, DRIFT spectra was collected to obtain the information about the adsorbed species. DRIFT spectra were recorded while ramping the temperature from 120 to 500 °C with

the interval of 50 °C in the lean gas atmosphere, which provided us with the desorption behavior of the adsorbed species. The reference spectrum was obtained at the same temperature during pretreatment process.

Inductively coupled plasma-atomic emission spectroscopy (ICP-AES) was conducted with Optima-4300 DV (PerkinElmer) to measure the amount of Pd in SSZ-13. Before analysis, 30 mg of samples was dissolved in aqua regia solution.

^{27}Al MAS (Magic angle spinning) Nuclear magnetic resonance (NMR) experiments were carried out on a 500 MHz WB Bruker Avance II system operating at 4 mm MAS probe. Spinning frequency of 10 kHz, a 65 kHz spectral window, 6572 complex points, and a 0.1 s pulse delay were utilized to acquire 512 time-averaged scans. Time domain free induction decays were apodized with exponential functions corresponding to 100 Hz of Lorentzian line broadening prior to Fourier transformation.

2.3. NO adsorption activity

An activity test was conducted in a quartz reactor. The catalyst (0.035 g) sieved between 150 and 180 μm was mixed with inert α-Al_2O_3 (0.1 g). The catalyst in the reactor was sustained at the same position by quartz wool. In front of the mixing line of gas mixture, water vapor (5%) was introduced by a syringe pump while heating the line at 120 °C. The total flow rate of the gases was 200 ml/min at a GHSV of 120,000 h^{-1}. A K-type thermocouple located on the top of the catalyst was used as the temperature of the reactor.

To simulate exhaust emission gas, CO_2 and H_2O were always introduced as reactant. Prior to NO adsorption, pretreatment was carried out at 500 °C with CO_2 (5%), H_2O (5%), and O_2 (9.5%) in N_2 for 30 min. For NO adsorption, 100 ppm of NO was introduced for 100 s with CO_2 (5%), H_2O (5%), and O_2 (9.5%) in N_2 at 120 °C. We tested NO adsorption at three temperatures such as 80, 120, and 160 °C. Among them, 120 °C shows the highest NO adsorption ability. After discussion with Hyundai-Kia motors company, 120 °C was selected as NO adsorption temperature. After the NO adsorption process with CO_2 (5%), H_2O (5%), and O_2 (9.5%) in N_2, the temperature of the catalyst was raised from 120 to 500 °C at a rate of 10 °C/min. The NO, NO_2, and NO_x concentration during temperature ramping were monitored by a NO_x analyzer (Thermo electron Corp., 42i-HL). To examine reproducibility of catalysts, each experiment was repeated at least 3 times, which is expressed by error bar in Fig. 2b. Note that most of our experiment conditions such as pretreatment and activity test are provided and/or determined by discussion with Hyundai-Kia Motors Company.

3. Results

3.1. Low temperature NO adsorption over various Pd/SSZ-13 catalysts

First of all, note that all NO species adsorbed on Pd/SSZ-13 are completely desorbed as NO or NO_2 below 500 °C based on the activity measurement results. The NO_x concentration and quantitative analysis during NO_x adsorption/desorption with and without catalyst are displayed in Fig. S1. The sum of unadsorbed NO_x during adsorption and desorbed NO_x during TPD is almost same as the amount of NO_x during blank test, so that it can be mentioned that the amount of NO adsorbed at 120 °C is almost equal to that of NO_x desorbed in the range of 120–500 °C. Hence, we regarded the latter amount as the NO adsorption capacity and also showed the NO_x desorption profile in the results part since the profile obtained during the temperature ramping provides more valuable information about the amount and strength of NO adsorption on Pd/SSZ-13.
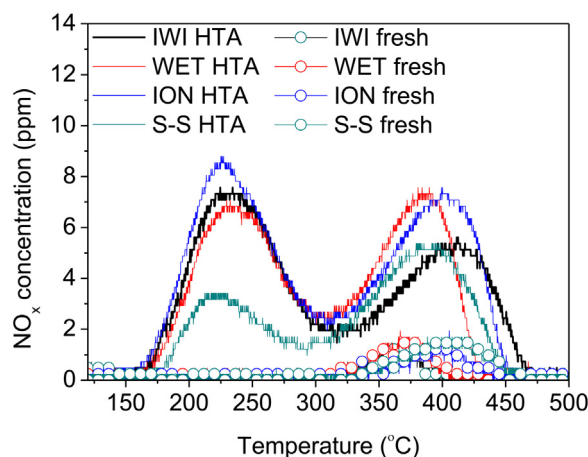

Fig. 1. NO_x desorption curves of fresh and HTA Pd(2)/SSZ-13 IWI, WET, S-S, and ION catalysts. NO adsorption temperature = 120 °C, ramping rate = 10 °C/min.

In order to investigate the effect of Pd loading methods on NO adsorption ability over the Pd(2)/SSZ-13 catalysts, various catalysts were prepared by applying four Pd loading methods such as IWI, WET, ION and S-S. Pd content (wt% and Pd/Al$_f$ ratio) determined by ICP analysis and NO adsorption capacity of the various Pd/SSZ-13 catalysts are listed in Table 1. Fig. 1 shows the NO_x desorption curves of fresh and HTA Pd(2)/SSZ-13 catalysts prepared by different synthesis methods after the adsorption of NO at 120 °C for 100 s. In addition, NO, NO_2, and NO_x concentration of HTA Pd(2)/SSZ-13 IWI during desorption are displayed in Fig. S2. It must be pointed out that regardless of various Pd loading methods, all of fresh Pd(2)/SSZ-13 catalysts hardly adsorb NO, as demonstrated by NO_x desorption profiles in Fig. 1 that shows only small trace of NO desorption at around 350 °C. In contrast, HTA Pd(2)/SSZ-13 catalysts clearly show two distinct desorption peaks having a maximum intensity at around 250 °C and 400 °C, indicating that HTA treatment allows all catalysts to have the improved NO adsorption ability. Furthermore, the fact that all HTA catalysts exhibit similar NO_x desorption profiles and, moreover, most of desorbed NO_x species (>95%) primarily consist of NO implies the existence of the similar NO adsorption sites irrespective of loading methods. However, although the Pd content of all catalysts is around 2 wt%, it must be pointed out that NO adsorption ability of each catalyst is slightly different depending on Pd loading method. Synthesis method using the aqueous solution (IWI; 26.2 μmol/gcat, WET; 25.8 μmol/gcat, and ION; 31.1 μmol/gcat) presents superior NO adsorption ability to S–S (17.1 μmol/gcat) method.

To obtain the information about the effect of Pd amount in SSZ-13 on NO adsorption/desorption, a series of fresh and HTA Pd(M)/SSZ-13 IWI (M: 0.2–5 wt%) were also evaluated. To facilitate the control of Pd loading, IWI method was adopted to load Pd on SSZ-13. Pd loadings and the amount of NO_x adsorbed of various catalysts are also listed in Table 1. NO_x desorption curves over the catalysts with the various Pd wt% loadings are displayed in Fig. 2a. In the HTA catalysts, an increase in the Pd loading yields an increase in NO adsorption capacity up to 2 wt% (Pd/Al$_f$: 0.3). As can be seen in Fig. 2a, Pd(0.2)/SSZ-13 IWI shows broad NO_x desorption feature from 150 to 450 °C. Above 0.5 wt% of Pd, the NO_x desorption peak of high temperature (at 400 °C) grows significantly and maintains similar intensities for the samples with higher Pd loading. In the case of the low temperature peak (at 250 °C), the NO adsorption capacity gradually increases up to 2 wt%, whereas it decreases at higher Pd content such as 3 and 5 wt% in comparison of HTA Pd(2)/SSZ-13. Fig. 2b shows the change in the NO adsorbed on HTA catalysts as a function of Pd amount. With increasing the amount of Pd from 0.2 to 0.5 wt%, the amount of
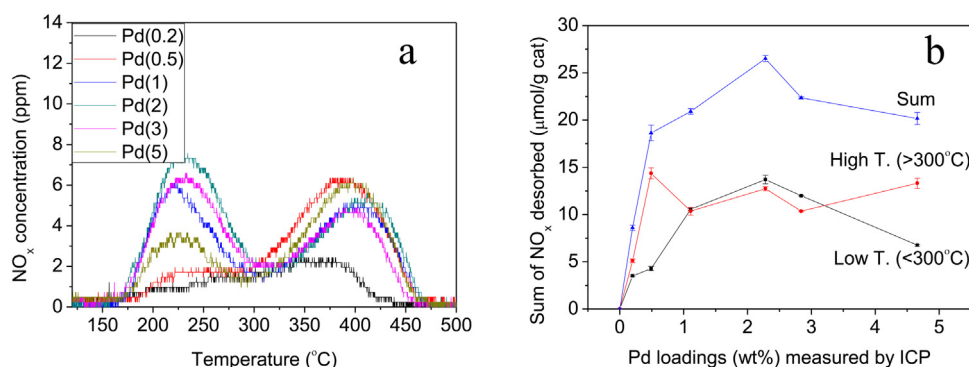
Fig. 2. NOx desorption (a) curves and (b) amount of HTA Pd/SSZ-13 IWI catalysts with various Pd loadings.

Table 1
Pd loadings (as synthesis) and NO adsorption capacity (after HTA) of Pd/SSZ-13 catalysts measured by ICP and NO adsorption/desorption experiment, respectively.

Catalyst		Pd content		NO adsorption capacity of HTA catalyst	
		Pd wt%	Pd/Al$_f$[a]	(μmol/gcat)[b]	(%)[c]
IWI[*]	Pd(5)	4.66%	0.61	20.2	30.7
	Pd(3)	2.84%	0.37	22.5	34.2
	Pd(2)	2.28%	0.30	26.2	40.0
	Pd(1)	1.11%	0.14	21.7	33.0
	Pd(0.5)	0.49%	0.06	19.4	29.6
	Pd(0.2)	0.20%	0.03	8.9	13.5
WET[*]	Pd(2)	2.35%	0.31	25.8	39.0
ION[*]	Pd(2)	2.04%	0.27	31.1	47.3
S-S[*]	Pd(2)	2.04%	0.27	17.1	26.0

[a] Framework Al.

[b] $\frac{the\ amount\ of\ NOx\ during\ TPD(\mu mol)}{the\ amount\ of\ catalyst\ used\ inex\ periment(g)}$

[c] $\frac{the\ amount\ of\ NOx\ during\ TPD(\mu mol)}{the\ amount\ of\ NOx\ during\ blank\ test(\mu mol)} \times 100$

[*] IWI: Incipient wetness impregnation, WET: Wet impregnation,, ION: Ion exchange, S-S: Solid-state ion exchange.

NO desorbed at high temperature considerably increases from 5.2 to 14.9 μmol/gcat and maintains similar capacity between 10.4 and 13.9 μmol/gcat at higher Pd loadings. However, in the case of the low temperature desorption peak, only small amount of NO adsorption capacity increases from 0.2 (3.6 μmol/gcat) to 0.5 (4.5 μmol/gcat) wt%. In contrast to high temperature desorption peak, the significant growth of NOx adsorption ability is observed at 1 (10.2 μmol/gcat) and 2 (14 μmol/gcat) wt% of Pd. However, 3 and 5 wt% Pd/SSZ-13 show the significant decrease in the amount of NO adsorption of 12.0 and 6.9 μmol/gcat, respectively. In summary, the peak area of low temperature NOx desorption (<300 °C) increases up to 2 wt% and decreases at above 3 wt%, whereas that of high temperature NOx desorption (>300 °C) exhibits similar NOx desorbed at above 0.5 wt% of Pd loading. Consequently, the sum of two desorption peaks shows volcano-shape curve with a maximum at 2 wt% (Fig. 2b, Sum), demonstrating that HTA Pd/SSZ-13 catalyst has optimum Pd loading for low temperature NO adsorption. Besides, the fact that the high temperature desorption peak is preferentially enhanced at lower Pd content (0.5 wt%) indicates that the NO adsorption site of high temperature is more readily activated than that of low temperature. Similar to other fresh catalysts, a negligible NO adsorption ability of fresh catalysts with various Pd loadings is observed (not shown). Thus, it can be concluded that the HTA treatment is an essential process to activate Pd/SSZ-13 to adsorb NO at low temperature.

3.2. XRD and NMR

XRD patterns of fresh and HTA Pd(2)/SSZ-13 IWI samples are shown in Fig. 3. Moreover, the XRD patterns in the region of PdO in Pd(M)/SSZ-13 IWI (M: 0.2–5 wt%) are shown in Fig. S3. Diffrac-
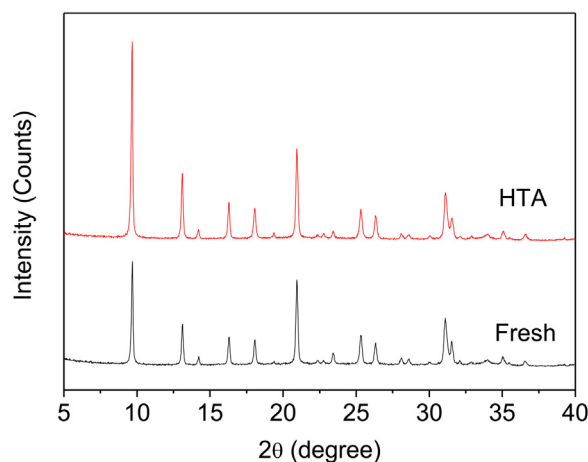

Fig. 3. XRD patterns of fresh and HTA Pd(2)/SSZ-13 IWI catalysts.

tion peaks of fresh Pd(2)/SSZ-13 sample are well matched with the Chabazite structure of SSZ-13 (JCPDS 52-0784). After hydrothermal aging treatment, although intensities of some peaks assigned to SSZ-13 increase slightly compared with fresh ones, the overall zeolite structure is maintained after HTA treatment. Note that bare SSZ-13 has a small diffraction peak at around 34° which is overlapped with that of crystalline PdO phase at 33.9° (JCPDS 43-1024). Such interference between PdO and SSZ-13 makes it difficult to accurately measure the peak intensity of PdO. However, in the Pd wt% ranging from 2 to 5, the increase in PdO peak intensity is clearly observed, demonstrating the growth of crystalline PdO depending on the amount of Pd in SSZ-13. Moreover, it is worth mentioning
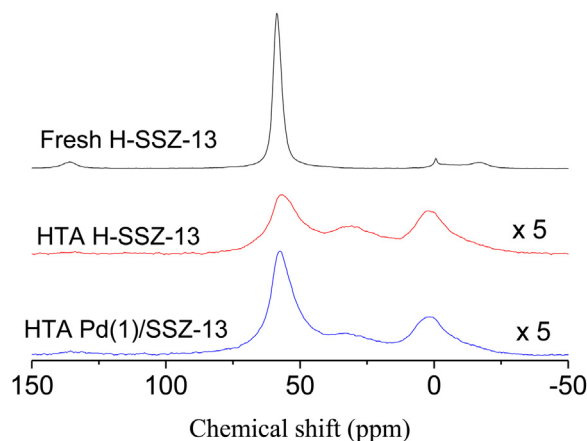
Fig. 4. Solid-state ^{27}Al-NMR spectra of fresh and HTA H-SSZ-13, and HTA Pd(1)/SSZ-13 IWI.

that there is no difference in the intensity of PdO peak between fresh and HTA samples except for Pd(5)/SSZ-13. In other words, the PdO peaks of Pd(2) and Pd(3)/SSZ-13 maintain its intensity even after HTA while only Pd(5)/SSZ-13 exhibits the growth of PdO peak, which provides the evidence that the sintering of PdO occurs significantly over Pd(5)/SSZ-13 resulting from HTA. Regardless of the amount of Pd loading, the remarkable change of SSZ-13 phase is not observed in any case, demonstrating that the zeolite structure of Pd/SSZ-13 catalysts is quite stable upon the hydrothermal aging treatment.

Hydrothermal aging on zeolite usually causes the extraction of Al element in the zeolite framework by hydrolysis (i.e. dealumination) without significant damage on their crystal structures. In order to investigate the dealumination of zeolite, ^{27}Al MAS NMR is carried out for fresh and HTA H-SSZ-13 with HTA Pd(1)/SSZ-13 IWI which is displayed in Fig. 4. The spectrum of fresh H-SSZ-13 exhibits an intense peak of the tetrahedrally coordinated framework Al located at ~58 ppm. A peak at 1 ppm is attributed to octahedrally coordinated Al in the fresh sample. After HTA treatment on H-SSZ-13 and Pd/SSZ-13, the significant decrease in the peak of tetrahedral framework Al and the appearance of penta- and octahedral Al peaks (centered at ~30 and ~1 ppm, respectively) are observed. Such results indicate the formation of extra framework AlO$_x$ species, resulting from dealumination of zeolite. One noticeable observation is that the peak area and intensity of tetrahedral Al in HTA Pd(1)/SSZ-13 is bigger than that of HTA H-SSZ-13, which implies that Pd containing sample has more Al sites in SSZ-13 framework after HTA treatment.

3.3. H$_2$-TPR and XPS

NO adsorption/desorption activity results allow us to confirm that HTA treatment activates the adsorption site of NO on Pd/SSZ-13. Moreover, since XRD results demonstrate the maintenance of zeolite structure during HTA, we pay more attention to the change in the nature of Pd on SSZ-13 after HTA.

H$_2$-TPR profiles of fresh and HTA Pd/SSZ-13 IWI catalysts are displayed in Fig. 5. All catalysts exhibit the release of physisorbed Ar in zeolite pore below − 50 °C [10]. Fresh Pd/SSZ-13 samples present a strong H$_2$ consumption peak at ca. 0 °C with a small minus peak at ca. 60 °C. Since H-SSZ-13 has only one desorption peak of Ar below − 50 °C (not shown), a positive and a negative feature of H$_2$ consumption over Pd/SSZ-13 are attributed to the presence of Pd. According to the previous study, a low temperature H$_2$ consumption around 0 °C is ascribed to the reduction of PdO to Pd and the formation from Pd to Pd hydride [10–12]. The minus feature at 60 °C originates from the decomposition of Pd hydride to release H$_2$, which is good agreement with previous studies [10,11,13]. In Fig. 5, the intensities of PdO reduction are linearly proportional to the amount of Pd in fresh Pd/SSZ-13, demonstrating that PdO exists primarily in fresh Pd/SSZ-13 samples.

However, hydrothermal treatment leads to a significant change in the reducibility of Pd in SSZ-13. Below 1 wt% of Pd, the peak intensity at ca. 0 °C is hardly shown after the HTA. Furthermore, the decomposition feature of Pd hydride disappears, indicating that most of Pd in HTA Pd(0.5 and 1 wt%)/SSZ-13 have a different nature from PdO in fresh ones. In addition, compared with fresh catalysts, a broad H$_2$ consumption peak from ca. 25–125 °C is noticeably observed. It is reported that Pd ions located in supercages of zeolite X and Y are reduced by H$_2$ at around 90 °C [12,13]. Furthermore, Sachtler et al. observed that the reduction peak of Pd ions in zeolite is located at much higher temperature (90–250 °C) than PdO with a broad feature [10,14,15]. Therefore, such observation provides the evidence of the presence of Pd ion species in HTA Pd/SSZ-13 samples.

With increasing Pd loadings to 2 and 3 wt% in HTA Pd/SSZ-13 sample, H$_2$ consumption peak of PdO comes to appear with a broader and smaller peak at higher temperature than that of fresh ones. Previous literature [11] reported that smaller PdO particle on zeolite support exhibits broader reduction peak at higher temperature (ca. 26 °C) than large PdO particle, which supports the formation of small PdO particles on Pd/SSZ-13 with high Pd loading after HTA treatment. Moreover, despite the peak overlapping between the Pd ion reduction and PdH$_x$ decomposition at higher Pd loading samples (2 and 3 wt%), we could observe the existence Pd ion over the HTA samples, as evidenced by the higher background in the range of 25–100 °C. Thus, H$_2$-TPR led us to confirm that HTA treatment induces the redispersion of bulk PdO into Pd ions, in addition to the formation of smaller PdO particle.
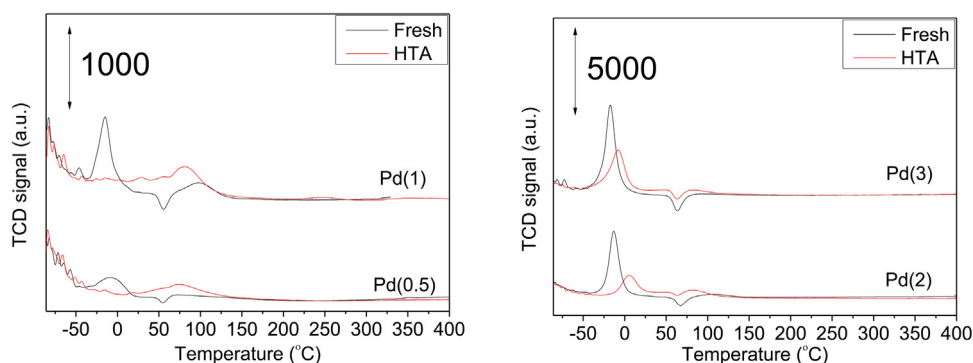

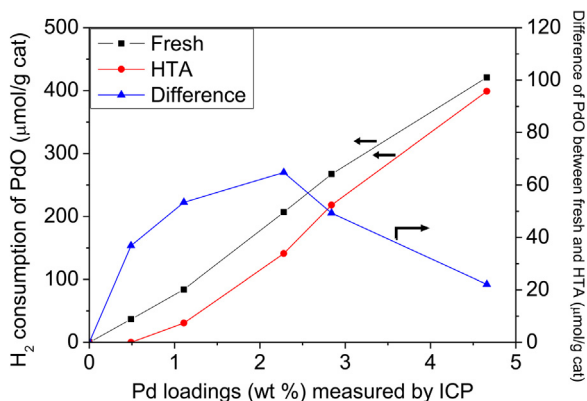**Fig. 5.** H$_2$-TPR spectra of fresh and HTA Pd/SSZ-13 IWI catalysts.

Fig. 6. Difference of the amount of PdO reduced at around 0 °C between fresh and HTA samples calculated by H_2-TPR of Pd/SSZ-13 IWI catalyst.
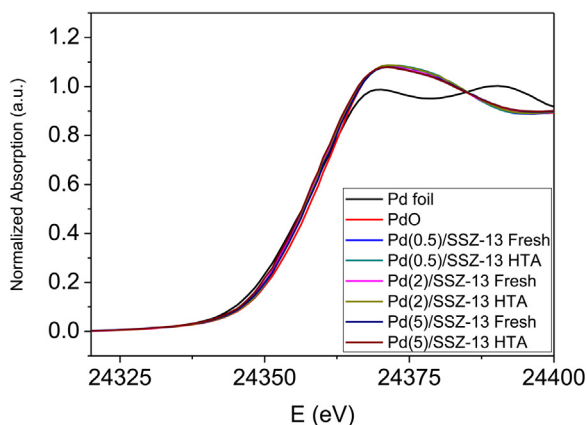

Fig. 7. Pd K edge XANES of fresh and HTA Pd(0.5, 2, and 5)/SSZ-13 IWI catalysts in addition to Pd foil and PdO.

Based on the quantitative analysis calculated by the numerical integration method, Fig. 6 exhibits the amount of H_2 consumption to reduce bulk PdO in Pd/SSZ-13 as a function of Pd wt%, in addition to the difference in the amount of H_2 consumed for bulk PdO reduction between fresh and HTA catalysts. As mentioned above, in the fresh catalysts, the amount of H_2 consumption to reduce PdO is almost equal to that of Pd in Pd/SSZ-13, while HTA samples show the relatively lower H_2 consumption, especially at low Pd loading. The difference in the amount of H_2 consumed to reduce PdO between fresh and HTA catalysts increases and reaches its maximum at 2 wt%.

In order to determine the Pd state in Pd/SSZ-13, XPS analysis is conducted. Fig. S4 shows the Pd 3d spectra of fresh and HTA Pd(1)/SSZ-13 IWI which display the same binding energy (BE) at 336.7 eV corresponding to the oxidation state of Pd^{2+}, demonstrating that the dominant oxidation state of Pd on SSZ-13 is Pd^{2+} before and after HTA treatment. In Fig. S4, one noticeable feature after HTA treatment is the significant decrease in the relative surface concentration of Pd from 0.99 to 0.38.

3.4. XAFS and STEM

Fig. 7 presents a series of selected Pd K-edge XANES spectra of fresh and HTA Pd/SSZ-13 IWI in addition to PdO and Pd foil as standards. For comparison, we selected specific Pd content such as low (0.5 wt%), middle (2 wt%), and high (5 wt%) concentration. In white line region, it is clear that the spectra of all Pd/SSZ-13 catalysts including Pd(1 and 3 wt%)/SSZ-13 (not shown) have similar shape with the spectrum of PdO, demonstrating that the dominant oxi-

dation state of all Pd species in SSZ-13 is +2 before and after HTA, which is well corresponding to the results of XPS.

Fourier transforms and oscillations of k^3-weighted EXAFS for fresh and HTA Pd/SSZ-13 IWI are displayed in Fig. 8 and Fig. S5, respectively. For comparison, the spectra of PdO and Pd foil are also included in Fig. 8. In the spectra measured before HTA (Fig. 8), two intense peaks appeared at ca. 1.5 and 3 Å (phase shift uncorrected) due to Pd-O bond and Pd-(O)-Pd, respectively, indicating the formation of bulk PdO, which is evident from the resemblance with the spectrum for PdO reference. The similar intensities of Pd-O bond at about 1.5 Å from 0.5 to 5 wt% imply the same oxidation state of Pd (+2) in all samples in spite of the different Pd loading. On the other hand, the peak intensity of Pd-(O)-Pd increases gradually with increasing the amount of Pd in SSZ-13. Since the intensity of Pd-(O)-Pd shells is related to the size of PdO [16], it can be inferred that the particle size of PdO in fresh samples increases with the amount of Pd.

No detectable change takes place in the Pd-O peaks after HTA treatment, whereas the intensity of Pd-(O)-Pd peak is significantly reduced especially at lower Pd content such as 0.5 and 1 wt%, implying the transformation of PdO into highly dispersed Pd^{2+} resulting from HTA treatment. Besides, it is noteworthy to point out that Pd-(O)-Pd shell is not observed in HTA Pd(0.5)/SSZ-13, which supports the presence of monodispersed Pd^{2+} ions in catalyst. Those results are well correlated with H_2-TPR result which shows the significant decrease in the reduction peak of bulk PdO as well as the appearance of the reduction peak of Pd ions after HTA.

For the case of Pd/SSZ-13 samples with 2 and 3 wt% Pd, the extent of peak reduction is not so big as the samples with lower Pd loadings, although the peak intensity of Pd-(O)-Pd decreases slightly after HTA treatment. Table 2 displays the coordination number (CN) and various parameter calculated by the basis of curve-fitting analysis. The CN of Pd-(O)-Pd shells for Pd(1)/SSZ-13 decreases from 2.8 ± 2.8 to 0.8 ± 1.2 after HTA, whereas, relatively, smaller change of CN is observed for Pd(2)/SSZ-13. This implies that the change in PdO size during HTA is related to the amount of Pd loading. With the Pd range of 0.5–3 wt% samples, even though the reduction of Pd-(O)-Pd peak is observed between fresh and HTA, the extent of peak reduction decreases with increasing the amount of Pd. Finally, Pd(5)/SSZ-13 shows the increase in Pd-(O)-Pd peak after HTA to the contrary, indicating the growth of PdO particle, which is good agreement with XRD result in Fig. S3.

To further visualize the effect of HTA on Pd in SSZ-13, the distribution of Pd was examined by STEM-EDS analysis before and after HTA treatment. Fig. 9 shows Pd EDS maps and Z-contrast STEM images over the fresh and HTA Pd(1)/SSZ-13 IWI. In Fig. 9a, fresh catalyst clearly exhibits several strong Pd signals (red spot) in patches. Moreover, in the same locations (red circle), dark contrasts are observed in the STEM image (Right, Fig. 9a), indicating that the formation of large Pd particles. Based on these observations, it could be claimed that Pd is locally agglomerated on the fresh sample. After activation by HTA, however, it is shown that Pd signals are homogeneously redistributed within the whole particle (in Fig. 9b), implying the formation of finely dispersed Pd species in HTA Pd(1)/SSZ-13 IWI. Although this result cannot be the direct evidence of the presence of Pd ion, it strongly supports the redistribution of bulk PdO in SSZ-13 resulting from HTA treatment.

3.5. DRIFT results during NO adsorption/desorption of HTA Pd(2)/SSZ-13

As described above, HTA treatment on Pd/SSZ-13 results in the redistributed Pd^{2+} ion species which is different from PdO of fresh sample. Moreover, such well-dispersed Pd^{2+} ion species are able to provide NO adsorption ability on Pd/SSZ-13 at low temperature. In order to have a better understanding of the origin of adsorption
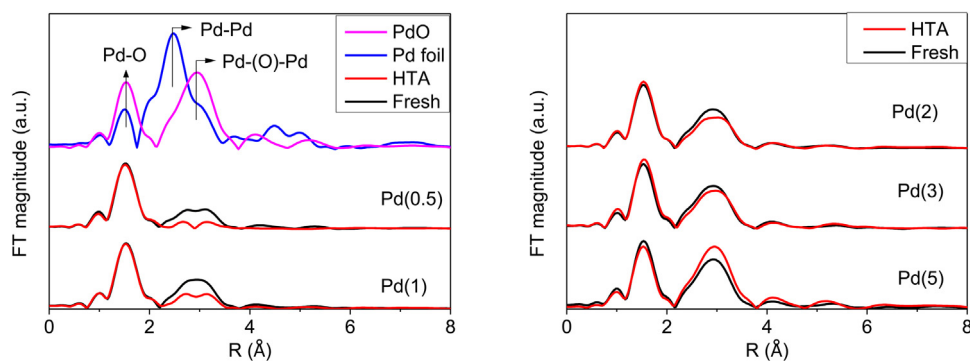
Fig. 8. Fourier transforms of k^3-weighted Pd K edge EXAFS for Pd metal, PdO, and Pd/SSZ-13 IWI with various Pd loadings.

Table 2
Results of curve fit of EXAFS data for Pd/SSZ-13 collected at Pd K edge.

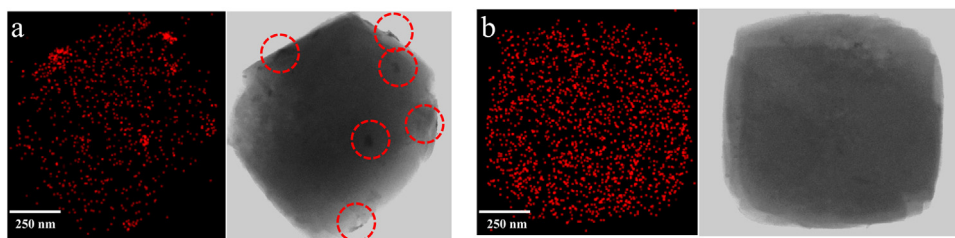| Pair	CN	Distance (nm)	DW factor (pm^2)	DE (eV)	R-factor
Fresh Pd(1)/SSZ-13 IWI					
Pd-O	3.1 ± 0.5	0.202 ± 0.001	7 ± 13	13.0 ± 1.5	0.018
Pd-Pd	**2.8 ± 2.8**	**0.307 ± 0.002**	64 ± 56		
HTA Pd(1)/SSZ-13 IWI					
Pd-O	3.8 ± 0.7	0.200 ± 0.001	21 ± 16	11.0 ± 0.0	0.058
Pd-Pd	**0.8 ± 1.2**	**0.306 ± 0.003**	46 ± 73		
Fresh Pd(2)/SSZ-13 IWI					
Pd-O	3.2 ± 0.5	0.202 ± 0.001	12 ± 14	12.7 ± 1.5	0.019
Pd-Pd	**4.2 ± 2.8**	**0.307 ± 0.001**	68 ± 38		
HTA Pd(2)/SSZ-13 IWI					
Pd-O	3.2 ± 0.5	0.201 ± 0.001	8 ± 14	12.0 ± 1.6	0.02
Pd-Pd	**3.2 ± 3.6**	**0.307 ± 0.002**	70 ± 63		

Fig. 9. (Left) EDS mapping analysis for Pd and (Right) Z-contrast STEM image of (a) fresh and (b) HTA Pd(1)/SSZ-13 IWI.

sites and the NO adsorption/desorption mechanism of HTA Pd/SSZ-13, a DRIFT study was performed after NO adsorption at 120 °C and the subsequent temperature ramping in a temperature range of 150–500 °C.

Fig. 10a exhibits the series of DRIFT spectra collected during NO/O$_2$ adsorption on HTA Pd(2)/SSZ-13 IWI in the presence of H$_2$O at 120 °C as a function of adsorption time in the range of 2000–1700 cm^{-1}. In addition, to investigate the origin of NO$_2$ desorbed at around 225 °C in Fig. S2, DRIFT spectra of HTA Pd(2)/SSZ-13 IWI is displayed in Fig. S6 in the range of 2000–1450 cm^{-1}. IR spectra of NO adsorbed HTA Pd(2)/SSZ-13 IWI obviously shows the highest peak at ca 1800 cm^{-1} with a shoulder at 1860 cm^{-1} both of which are assigned to nitrosyl complex on ionic Pd species [2,6,9,17,18], evidently supporting the presence of Pd^{2+} ion in SSZ-13. Besides, the peak at 1524 cm^{-1} is observed in Fig. S6 which is assigned to nitrite species.

On the basis of NO desorption experiment, there are two desorption peaks which primarily desorb as NO at low temperature (around 250 °C) and high temperature (around 400 °C). In order to identify the origin of NO$_x$ desorption at each temperature, it is important to analyze the behavior of the adsorbed NO$_x$ species during temperature ramping. Hence, after NO adsorption at 120 °C, the series of DRIFT spectra were acquired while raising the temperature

by 50 °C from 120 to 500 °C to understand the NO$_x$ desorption process. Fig. 10b exhibits the DRIFT spectra of HTA Pd(2)/SSZ-13 IWI as a function of temperature with the IR range of 2000–1700 cm^{-1}. Firstly, the elimination of the peak at 1524 cm^{-1} is observed at around 200 °C (data not shown), indicating that the NO$_2$ species in Fig. S2 arise from the nitrite species at 1524 cm^{-1} in Fig. S6. With the increase in temperature from 120 to 300 °C, the band at 1800 cm^{-1} rapidly decreased. Furthermore, it must be pointed out that the band at 1860 cm^{-1} gradually increases and eventually reaches its maximum at 300 °C. Above 300 °C, ionic Pd-NO species at 1860 cm^{-1} begin to decrease simultaneously with the reduction of the peak at 1800 cm^{-1}.

4. Discussion

4.1. The change in Pd species during HTA treatment

H$_2$-TPR analysis indicates that the main Pd species in fresh Pd/SSZ-13 are PdO. As mentioned in the introduction, NO is hardly adsorbed on PdO [4,19], providing the solid reason why fresh Pd/SSZ-13 catalysts cannot adsorb NO. However, after HTA treatment, the reduction behavior of Pd in SSZ-13 is significantly changed. The difference in the amount of PdO reduced between
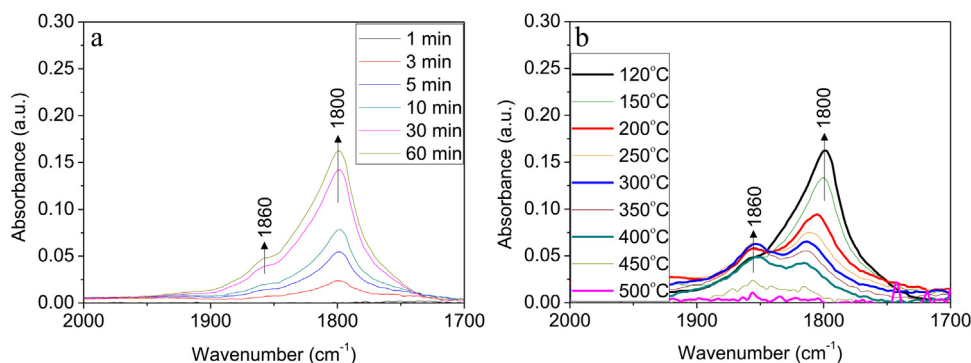
Fig. 10. DRIFT spectra during NO (a) adsorption as a function of time (min) and (b) desorption as a function of temperature (°C) over HTA Pd(2)/SSZ-13 IWI.

fresh and HTA samples increases up to 2 wt% and decreases at higher Pd wt% (in Fig. 6), which is similar to the trend of NO adsorption ability for HTA Pd/SSZ-13 IWI as a function of Pd loadings (in Fig. 2). It strongly implies that a close relationship exists between NO adsorption capacity and the amount of Pd species which are not reduced like bulk PdO in HTA Pd/SSZ-13. In addition, HTA Pd/SSZ-13 catalysts having NO adsorption ability exhibit the broad H_2 reduction peak of Pd ion species in H_2-TPR, indicating the formation of ionic Pd in HTA Pd/SSZ-13 samples. The presence of Pd ion as an active site of NO adsorption is clearly confirmed by DRIFT spectra of HTA Pd(2)/SSZ-13 IWI. After NO adsorption, HTA Pd(2)/SSZ-13 IWI exhibit two different peaks at 1800 and 1860 cm^{-1} assigned to nitrosyl complex on ionic Pd species. Considering the change in DRIFT peak with respect to the NO_x desorption curve in Fig. 1, it is obvious that the desorption of NO between 120 and 300 °C is related to the nitrosyl complex at 1800 cm^{-1} and NO desorption peak at high temperature originates from ionic Pd-NO species observed at 1860 cm^{-1}. Therefore, it can be mentioned that Pd ions in SSZ-13 induced by HTA treatment play as an active site for NO adsorption at low temperature. In addition, both XPS and XANES results of HTA Pd/SSZ-13 support that the oxidation state of the transformed Pd species is 2+, indicating the formation of Pd^{2+} ions in catalyst after HTA treatment.

The formation of Pd^{2+} ion in SSZ-13 results from the redistribution of Pd species during HTA treatment. In XPS analysis, the relative surface concentration of Pd in Pd(1)/SSZ-13 decreases significantly after HTA, implying the mobility of Pd species from surface to inside SSZ-13. Furthermore, the decrease in the intensity of Pd-(O)-Pd shell at low Pd content such as 0.5 and 1 wt% was observed in EXAFS analysis (in Fig. 8). Since the Pd-(O)-Pd shell reflects the formation of PdO species, the reduced intensity of Pd-(O)-Pd demonstrates the transformation of PdO into highly dispersed Pd^{2+}, which also provides evidence about Pd redispersion in Pd/SSZ-13 during HTA. In addition, by visualizing agglomerated and well dispersed Pd species in fresh and HTA Pd(1)/SSZ-13 IWI, respectively, STEM-EDS also shows the redistribution of Pd. In summary, HTA treatment induces the mobility of Pd on SSZ-13, leading to the redistribution of Pd species and formation of Pd ion in SSZ-13.

The combined results of H_2-TPR, XAFS, XPS, and DRIFT clearly confirm the generation of Pd^{2+} ion in SSZ-13, which leads us to conclude that HTA treatment induces the ion exchange of Pd^{2+} ions in SSZ-13. Such phenomenon is also reported by Wang et al. [20] who demonstrated that CuO species in the fresh precipitated catalyst migrate into the SAPO-34 during the HTA treatment and form isolated Cu ions at ion exchange site. They claimed that the reduction of CuO by high temperature (700 °C) is required for the ion exchange of Cu species. In case of Pd/SSZ-13, however, the role of H_2O is essential for the ion exchange of Pd. It is worth noticing that thermally treated Pd(2)/SSZ-13 IWI (750 °C, 25 h without H_2O) shows negligible NO adsorption ability (almost same as the fresh

samples, not shown), indicating that Pd ion exchange is not successful after HTA treatment in the absence of H_2O. Shwan et al. reported that Cu ion exchange in CuO/SSZ-13 takes place under specific gas compositions (NO and NH_3) at 250 °C [21]. They demonstrated that there are two key factors for ion exchange from CuO to Cu ion in SSZ-13. One is the reduction of CuO by NO molecule and another is the facilitation of mobility by forming $[Cu^1(NH_3)_x]^+$ ($x \geq 2$) complex. Similarly, it can be hypothesized that H_2O facilitates the mobility of Pd species at 750 °C, resulting in Pd redistribution and cation exchange in SSZ-13, which requires further analysis.

4.2. The effect of Pd ion exchange methods on the physicochemical state of Pd/SSZ-13

An insignificant NO adsorption ability of fresh Pd(2)/SSZ-13 ION obviously indicate that the main Pd species in the sample is PdO. This result clearly demonstrates the failure of cation exchange in SSZ-13 with ion exchange method. It is reported that the hydrolysis of metal ion must be prevented to introduce metal ions in zeolite by applying conventional ion exchange [22]. However, since hydrolysis of Pd ion in aqueous solution is started at low pH (below 2) [23,24], therefore, it is expected that the Pd ion is hydrolyzed during ion exchange procedure, resulting in the unsuccessful Pd cation exchange. In the case of medium and large pore zeolite such as ZSM-5, X, and Y, tetraammine palladium(II) ion ($Pd(NH_3)_4^{2+}$) species are generally applied [7,25–27]. However, since the diameter of $Pd(NH_3)_4^{2+}$ could be estimated to be roughly 7.5 Å which is larger than the aperture of SSZ-13 [28], the ion exchange of Pd ion does not take place. We also confirmed no activity of fresh Pd/SSZ-13 catalyst prepared by ion exchange method using $Pd(NH_3)_4^{2+}$ species as a Pd ion (not shown). Solid-state ion exchange does not occur successfully similar to ION sample, as verified by negligible NO adsorption ability in fresh Pd(2)/SSZ-13 S-S. Previous literature reported that solid-state ion exchange takes place through the gas phase transport of $PdCl_2$ [13]. However, since gaseous molecule is presumably Pd_6Cl_{12} whose size is approximately 7.6 Å [13], the introduction of the Pd precursor in SSZ-13 is also prevented by small pore size of SSZ-13 (3.8 Å). In summary, it can be mentioned that normal ion exchange of Pd in SSZ-13 by conventional method is difficult because of the hydrolysis of Pd ion and small pore structure of SSZ-13. Therefore, the formation of Pd^{2+} ion in SSZ-13 by HTA treatment can be regarded as the novel method for the ion exchange of Pd in small pore zeolite such as SSZ-13.

4.3. The limit of Pd ion exchange in SSZ-13 by HTA treatment

In NO adsorption/desorption experiment (3.1 section), it is confirmed that Pd/SSZ-13 with 0.3 of Pd/Al_f ratio (i.e. Pd 2 wt%) has the highest NO adsorption ability. In general, since the oxidation state of Pd after HTA is +2, as evidenced by XPS and EXAFS, the opti-
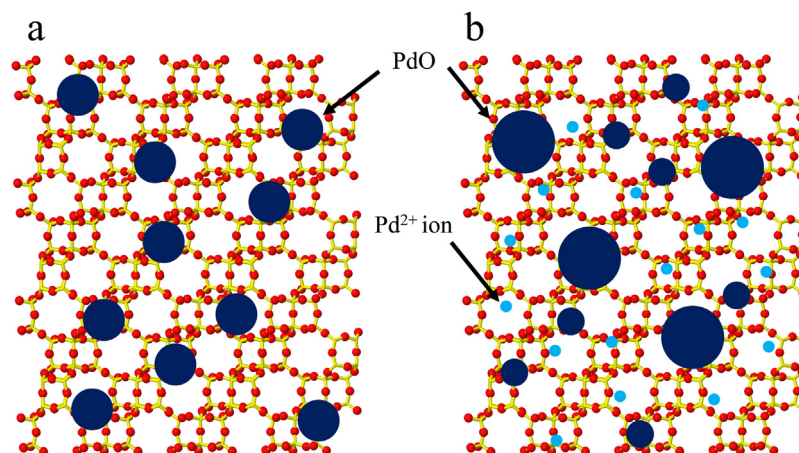
Fig. 11. Schematic model to represent the change in the nature of Pd (a) before and (b) after HTA treatment.

mum Pd/Al_f ratio would be 0.5 which is equivalent with 3.8 wt% of Pd. In addition, even though 2.28 wt% of Pd (measured by ICP, 214 μmol Pd/gcat) exhibits the highest NO adsorption ability, PdO species coexist with Pd^{2+} ion in HTA Pd(2)/SSZ-13 IWI catalyst, as verified by H_2-TPR which Exhibits 205 and 141 μmol/gcat of PdO reduction in fresh and HTA samples, respectively. To estimate the exact amount of Pd ion in HTA Pd(2)/SSZ-13 IWI, titration of Pd ion is carried out by using NO-TPD. In the previous literature, the measurement of metal ion such as Pd and Cu by NO molecule was reported by using 1:1 ratio of metal cation:NO [4,29]. In this work, since Pd ion-nitrosyl complex is mainly formed during NO adsorption, it can be assumed that the NO is able to adsorb on Pd ion at 1:1 stoichiometry. After NO adsorption for 1 h (i.e. until the saturation of Pd ion with NO molecule), NO-TPD was conducted with similar method to NO adsorption/desorption experiment, which is displayed in Fig. S7. As a results of titration, it was found that the amount of Pd ions capable of adsorbing NO is 50 μmol/gcat, which is similar to the amount of reduced PdO species measured by H_2-TPR before and after HTA (205 (fresh) − 141 (HTA) = 64 μmol/gcat). This result indicates that only 23% of Pd in Pd(2)/SSZ-13 IWI is converted to Pd ion species during HTA treatment. Such ion exchange level of Pd in SSZ-13 is explained by the limited number of ion exchange sites arising from the effect of hydrothermal treatment on SSZ-13. In NMR analysis, it is confirmed that the dealumination of SSZ-13 occurs significantly during hydrothermal treatment, resulting in the reduction of the number of framework Al sites. Therefore, it is reasonable to claim that dealumination of SSZ-13 leads to the lower number of ion exchange Al sites than theoretical one. Such decrease in the number of Al site in zeolite could explain the reason why Pd is not fully ion exchanged in SSZ-13 during HTA.

4.4. The effect of hydrothermal treatment on Pd/SSZ-13

In order to describe the effect of HTA treatment on Pd/SSZ-13, we propose the model for the nature of Pd species before and after HTA treatment as shown in Fig. 11. In the case of Cu-SSZ-13, there are two ion exchange sites for Cu ion in SSZ-13 such as 6-member ring and large cages associated with 8-member ring in SSZ-13 according to the previous literature [30–32]. However, we do not have enough information to determine the position of Pd ion in SSZ-13, therefore, Pd ion in Fig. 11b is randomly located in the possible ion exchange site. In the case of fresh Pd/SSZ-13, since Pd is not readily located into the ion exchange in SSZ-13 prepared even by ion exchange method, therefore, the principal Pd state in fresh catalysts is PdO. However, HTA treatment provides the mobility of PdO, resulting in the redistribution of Pd species within the zeolite. As a

result, it is found that HTA Pd(0.5)/SSZ-13 possesses the monodispersed Pd^{2+} ion species on the basis of H_2-TPR and Pd EXAFS. When Pd loading increases from 1 to 3 wt%, the shortage of ion exchange sites in SSZ-13 arising from dealumination leads to the limited Pd ion exchange, resulting in the observation of small PdO particle compared to the fresh catalysts. Thus, small PdO particle exists together with Pd^{2+} ion species in SSZ-13. At higher Pd loading sample such as Pd(5)/SSZ-13, redispersion and sintering of Pd take place simultaneously. In the H_2-TPR result, HTA Pd(5)/SSZ-13 shows the decrease in the amount of H_2 consumed to reduce bulk PdO. Furthermore, it has NO adsorption ability at low temperature. On the other hand, XRD and XAFS results clearly demonstrate the sintering of PdO during HTA treatment. Such contradictory results can be explained by the co-existence of Pd^{2+} ion and large PdO particles in HTA Pd(5)/SSZ-13. Therefore, in the case of HTA Pd(5)/SSZ-13, there are three kinds of Pd species which are Pd^{2+} ion, small PdO, and large PdO. In addition, based on the fact that HTA Pd(5)/SSZ-13 exhibits relatively lower NO adsorption ability than that of HTA Pd(2)/SSZ-13, it is expected that the sintering of PdO occurs more dominantly than the activation in SSZ-13 during HTA. Such assumption could be one reason for the presence of optimum Pd content in HTA Pd/SSZ-13 for low temperature NO adsorption. It can be summarized that the relative distribution of three different Pd species is totally depending on the amount of Pd in HTA Pd/SSZ-13 IWI sample.

5. Conclusion

The influence of HTA treatment on the adsorption of NO at low temperature over Pd/SSZ-13 has been extensively investigated. It is found that the ion exchange of Pd in SSZ-13 is rather difficult with any methods, probably due to the hydrolysis of Pd ion and the small pore structure of SSZ-13. The primary state of Pd in fresh catalyst is PdO, on which NO rarely adsorb, resulting in the insignificant NO adsorption ability of fresh catalyst. After HTA treatment at 750 °C for 25 h, Pd/SSZ-13 shows the enhanced NO adsorption ability at 120 °C. Such HTA catalysts exhibit two NO desorption features at around 250 and 400 °C. Moreover, NO adsorption ability of Pd/SSZ-13 increases from 0.2 to 2 wt% of Pd, whereas it decreases at higher Pd loading than 2 wt%. NO adsorption/desorption results lead us to confirm that HTA treatment is an essential process to yield an active catalyst for low temperature NO adsorption.

XRD patterns shows that the zeolite structure remains unchanged for all the Pd/SSZ-13 catalysts during HTA, whereas combined H_2-TPR and XAFS analysis clearly demonstrates that HTA treatment induced the transformation of bulk PdO into Pd^{2+} ion

in zeolite. Such change in the Pd dispersion is visually verified by STEM-EDS analysis which shows the agglomerated and well dispersed Pd species in fresh and HTA sample, respectively. Consequently, DRIFT spectra prove the presence of two kind of ionic Pd-NO species in HTA Pd(2)/SSZ-13 after NO adsorption. Taken together, DRIFT and NO adsorption/desorption results reveal that low temperature NO desorption peak (at 250 °C) arises from the ionic Pd-NO species (band at 1800 cm^{-1}), whereas another nitrosyl complex with Pd^{2+} ion at 1860 cm^{-1} is the major species to desorb NO at ca. 400 °C. In conclusion, HTA treatment on Pd/SSZ-13 provides the mobility of PdO leading to the redistribution to generate the Pd^{2+} ion species in SSZ-13 zeolite, which play as an active site for NO adsorption at low temperature.

Acknowledgments

Appendix A. Supplementary data

Supplementary data associated with this article can be found, in the online version, at http://dx.doi.org/10.1016/j.apcatb.2017.04.077.

References

[1] H. Chen, S. Mulla, E. Weigert, K. Camm, T. Ballinger, J. Cox, P. Blakeman, SAE Int. J. Fuels Lubr. 6 (2013) 372–381.
[2] H.Y. Chen, J.E. Collier, D.X. Liu, L. Mantarosie, D. Duran-Martin, V. Novak, R.R. Rajaram, D. Thompsett, Catal. Lett. 146 (2016) 1706–1711.
[3] T.M. Yuichiro Murata, Katsuji Wada, Hiroshi Ohno, SAE Int. J. Fuels Lubr. 8 (2015) 454–459.
[4] M. Ogura, M. Hayashi, S. Kage, M. Matsukata, E. Kikuchi, Appl. Catal B 23 (1999) 247–257.
[5] J. Rasko, F. Solymosi, J. Chem. Soc. Farad T 1 (80) (1984) 1841–1853.
[6] K. Chakarova, E. Ivanova, K. Hadjiivanov, D. Klissurski, H. Knozinger, Phys. Chem. Chem. Phys. 6 (2004) 3702–3709.
[7] C. Descorme, P. Gelin, M. Primet, C. Lecuyer, Catal. Lett. 41 (1996) 133–138.
[8] B. Pommier, P. Gelin, Phys. Chem. Chem. Phys. 3 (2001) 1138–1143.
[9] K.I. Hadjiivanov, Catal. Rev. 42 (2000) 71–144.
[10] B.J. Adelman, W.M.H. Sachtler, Appl. Catal. B 14 (1997) 1–11.
[11] S.B.C. Pergher, R.M. Dallago, R.C. Veses, C.E. Gigola, I.M. Baibich, J. Mol. Catal. A-Chem. 209 (2004) 107–115.
[12] H. Matsumoto, S. Tanabe, J. Mater. Sci. Lett. 11 (1992) 623–626.
[13] C. Stolz, A. Sauvage, P. Massiani, R. Kramer, Appl Catal. A-Gen. 167 (1998) 113–121.
[14] O.C. Feeley, W.M.H. Sachtler, Appl. Catal. 75 (1991) 93–103.
[15] S.T. Homeyer, W.M.H. Sachtler, Appl. Catal. 54 (1989) 189–202.
[16] K. Okumura, J. Amano, N. Yasunobu, M. Niwa, J. Phys. Chem. B 104 (2000) 1050–1057.
[17] F. Lonyi, H.E. Solt, J. Valyon, H. Decolatti, L.B. Gutierrez, E. Miro, Appl. Catal. B 100 (2010) 133–142.
[18] K. Shimizu, F. Okada, Y. Nakamura, A. Satsuma, T. Hattori, J. Catal. 195 (2000) 151–160.
[19] J.M. Watson, U.S. Ozkan, J. Catal. 210 (2002) 295–312.
[20] L. Wang, J.R. Gaudet, W. Li, D. Weng, J. Catal. 306 (2013) 68–77.
[21] S. Shwan, M. Skoglundh, L.F. Lundegaard, R.R. Tiruvalam, T.V.W. Janssens, A. Carlsson, P.N.R. Vennestrom, ACS Catal. 5 (2015) 16–19.
[22] L. Guczi, I. Kiricsi, Appl. Catal. A-Gen. 186 (1999) 375–394.
[23] L.A. Koroleva, N.D. Shikina, P.G. Kolodina, A.V. Zotov, B.R. Tagirov, Y.V. Shvarov, V.A. Volchenkova, Y.K. Shazzo, Geochem. Int. 50 (2012) 853–859.
[24] C.F. Baes, Reprint ed., The hydrolysis of cations, Malabar, Fla.: R.E. Krieger, 1986., Malabar, Fla., 1986.
[25] L. Becker, H. Forster, Appl. Catal. B 17 (1998) 43–49.
[26] Z. Karpinski, S.N. Gandhi, W.M.H. Sachtler, J. Catal. 141 (1993) 337–346.
[27] P. Gallezot, Catal. Rev. 20 (1979) 121–154.
[28] B. Pommier, P. Gelin, Phys. Chem. Chem. Phys. 1 (1999) 1665–1672.
[29] Y.J. Kim, J.K. Lee, K.M. Min, S.B. Hong, I.S. Nam, B.K. Cho, J. Catal. 311 (2014) 447–457.
[30] D.W. Fickel, J.M. Fedeyko, R.F. Lobo, J. Phys. Chem. C 114 (2010) 1633–1640.
[31] U. Deka, A. Juhin, E.A. Eilertsen, H. Emerich, M.A. Green, S.T. Korhonen, B.M. Weckhuysen, A.M. Beale, J. Phys. Chem. C 116 (2012) 4809–4818.
[32] J.H. Kwak, T. Varga, C.H.F. Peden, F. Gao, J.C. Hanson, J. Szanyi, J. Catal. 314 (2014) 83–93.